Electrical, Transport and Optical Properties of Multifunctional Graphitic Films Synthesized on Dielectric Surfaces by Nickel Nanolayer Assisted Pyrolysis

Marian Baah,[1] Petr Obraztsov,[2] Alesia Paddubskaya,[3] Andrius Biciunas,[4] Sari Suvanto,[5] Yuri Svirko[1], Polina Kuzhir [1,3,], and Tommi Kaplas[1,4]*

[1]Institute of Photonics, University of Eastern Finland, Yliopistokatu 7, FI-80101 Joensuu, Finland

[2] Prokhorov General Physics Institute, RAS, 38 Vavilov st., Moscow, 119991, Russia

[3]Institute for Nuclear Problems of Belarusian State University, Bobruiskaya 11, 220030 Minsk

[4]Center for Physical Sciences and Technology, Saulėtekio av. 3, LT-10257 Vilnius, Lithuania

[5]Department of Chemistry, University of Eastern Finland, Yliopistokatu 7, FI-80101 Joensuu, Finland

*corresponding author: polina.kuzhir@uef.fi

Abstract

We demonstrate that predepositing on the dielectric surface a nanometrically thin nickel film is sufficient to transform amorphous pyrolyzed photoresist film (PPF) into a graphitic film (GRF) enriched with nickel particles. The GRF shows three orders of magnitude higher carrier mobility than that of amorphous PPF, while its electrical conductivity doubles after etching away the nickel remains. The pronounced 2D peak in the Raman spectrum, almost dispersionless absorbance in the spectral range of 750 – 2000 nm, and saturable absorption coefficient indicate that GRF possesses graphene-like band structure. The proposed cost-efficient and scalable synthesis route opens avenues towards fabrication of micron size patterned graphitic structures of any shape directly on a dielectric substrate. Having graphene-like transport and electrical properties at the 20 times higher absorbance than the single layer graphene, GRF is attractive for fabrication of fast modulators of optical radiation, bolometers and other photonics and optoelectronic devices that require an enhanced optical absorption.
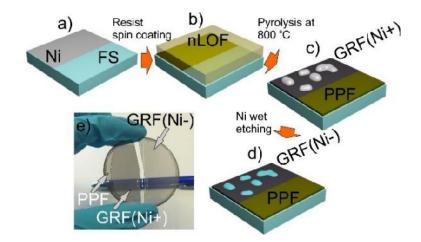
1. Introduction

The dispersionless absorption coefficient of graphene in the VIS-NIR spectral range[1, 2] makes this 2D material attractive for a number of optoelectronic applications. However, being atomically thin, an isolated graphene sheet absorbs only 2.3% of the incident electromagnetic radiation that is not enough for using it in photodetectors or modulators that require materials with higher optical absorption ability. There exist several techniques that enable the enhancement of the graphene absorption whilst preserving high carriers mobility and mean free path, e.g. by organizing graphene nanosheets into vertically oriented array made by plasma-enhanced chemical vapor deposition (see[3] and Ref.[4] for comprehensive review), by modifying the substrate[5] or patterning the graphene[6]. However, replacing graphene with a graphitic film (GRF) comprising of several

graphene layers may be a simpler solution, because its absorbance is solely determined by the number of graphene sheets. It has already been demonstrated[7] that GRF may be attractive for a number of photonic and optoelectronic applications. For instance, the saturable absorption in the GRF deposited on a dielectric substrate enables mode locking and generation of ultrashort pulses in the fiber and solid state lasers[8]. Nonetheless the deposition of a thin layer of crystalline graphite (or multilayer graphene) on a dielectric substrate is still challenging task. This is because the fabrication of GRF is conventionally based on the chemical vapor deposition (CVD) on metallic (e.g. nickel or copper) transient substrates[9, 10], while photonic and optoelectronic applications usually require dielectric ones. The necessity to transfer GRF from metal to dielectric substrate significantly hampers their use in practice. Although recently a substantial progress has been made in transferring graphene[11], the most appealing would be to grow GRF directly on dielectric support.

The direct growth of continuous graphene on the insulating support has been demonstrated on the molten glass that enables a highly uniform graphene nucleation[12]. Another approach suggests using a dielectric substrate with a pre-deposited few hundred nanometers thick sacrificial copper layer[13-15]. However, this technique allows one to obtain a monolayer or a very few graphene sheets deposited on the dielectric substrate, whereas the problem of the thicker GRF deposition on dielectric support still remains unresolved.

The eagerly awaited by photonic and optoelectronic community solution of this problem implies finding a feasible alternative to CVD technique. In this respect recently proposed[16] pyrolysis of the photoresist film in presence of a nanometrically thin nickel layer deserves attention. Specifically, it has been shown that pyrolysis at the temperature of 800 °C transforms several hundred nanometers thick photoresist layer into tens of nanometers thick GRF embedded with Ni nanoparticles[16]. Such an ultra-thin GRFs have already exhibited an impressive performance in the surface enhanced Raman spectroscopy and nonlinear optics[16, 17], although relationship between their properties and synthesis conditions are still unclear.

In this paper, we report an extensive investigation of the optical and transport properties of GRF synthetized on SiO_2 by using a nanometrically thin sacrificial nickel layer. We demonstrate that by pre-depositing 10 nm thick layer of Ni catalyst on the silica substrate one can transform amorphous pyrolyzed photoresist film (PPF) into GRF embedded with Ni nanoparticles, which can be readily etched away after the synthesis. Such a drastic impact of the Ni film on the pyrolysis of the photoresist opens avenues towards new approach for the synthesis of graphitic films and their application in photonic and optoelectronic devices. We report here an extensive comparative study of physical properties of GRFs with and without Ni particles, and show that removal of Ni nanoparticles does not affect crystallinity of the film. Thus, we propose an appealing route to produce micron size graphitic structures that can be utilized for scalable fabrication of graphitic circuits on a dielectric substrate.

2. Samples fabrication

We fabricated GRF on silica substrate by nickel catalyst-assisted pyrolysis of photoresist at elevated temperature. A part of a silica substrate was coated by ten nanometers thick Ni catalyst layer, which was thermally evaporated on a substrate (by Leybold Univex 300). After that the sample was spin coated with 350 nm thick resist layer (AZ 2070 nLOF diluted with AZ EBR in the ratio 1:4). The spin coated resist film was pre-baked for 1 min at 110 °C.

Figure 1: A schematic illustration of the process flow to synthetize GRF on a dielectric substrate. (a) A layer of GRF was synthetized by covering a dielectric substrate with a thin Ni film and (b) with a nLOF resist film. (c) Annealing the sample in elevated temperature activate the catalysis resulting GRF with Ni particles (GRF(Ni+)). Areas without Ni film were coated with amorphous pyrolyzed photoresist film (PPF). (d) Nickel remains can be then removed by wet etching, which results graphitic film without Ni particles (GRF(Ni-)). (e) An image of a two-inch fused silica substrate; one-half covered with GRF(Ni+) and second half with GRF(Ni-).

The substrate with sacrificial Ni nanolayer and spin-coated resist film was then annealed in a CVD chamber at 800 °C in H_2 atmosphere (20 sccm / 1 mbar) for 10 minutes (see[16] for further details). By performing pyrolysis at different thicknesses of the Ni layer we revealed that in our experimental conditions, the optimal thickness of the Ni layer is 10 nm. At this thickness, the synthesized GRF film resembles the multilayered graphene in terms of crystallinity, thickness and surface conductivity yet showing mechanical robustness and a good adhesion to the dielectric support.

Although the pyrolysis of the photoresist film takes place already after 600 °C[16, 18], the Ni-assisted transformation of the PPF into GRF is activated once the temperature reaches 700 − 800

°C range. We observed evaporation of the solvent from the resist layer at temperature of 700 °C. At the same temperature the Ni film recedes forming sub-micron size Ni islands (see Fig. 1).

We believe that in presence of Ni nanolayer, the converting of a resist film to GRF is governed by the same mechanism as the chemical vapor deposition of the multilayer graphene on nickel foil[19]. Namely, at the temperature above 700 °C, the 10 nm thick nickel layer recedes forming particles of several hundred to several tens of nm, while the solubility of carbon in nickel sharply increases[20] leading to the saturation of the Ni islands with carbon atoms. Cooling nickel particles saturated with carbon atoms leads to the precipitation of graphene layers at the Ni surface[21] forming a homogeneous graphitic film with Ni particles embedded.
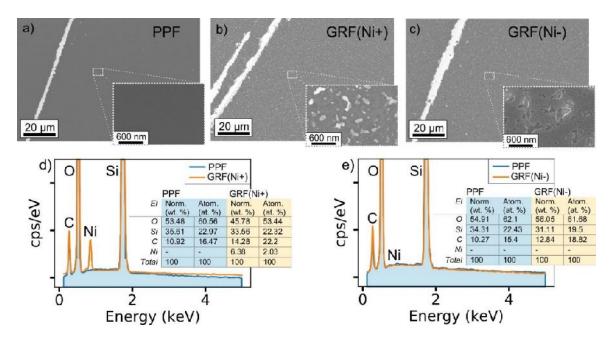
We perform comparative study of the photoresist films pyrolyzed without and with predeposited Ni catalyst at the same process conditions. The former are conventional PPFs, while the latter, which will be referred to as GRF(Ni+), are GRFs embedded with Ni nanoparticles (see Fig.1c). From one of the GRF samples we removed Ni particles by applying a brief oxygen plasma treatment (15 s / 20 sccm / 100 W) followed by the wet etching in $CuSO_4:HCl:H_2O$ solution (10 g:50 ml:50 ml). The GRF without Ni is denoted as GRF(Ni-)).

PPF, GRF(Ni+) and GRF(Ni-) were characterized by scanning electron microscopy (SEM - LEO 1550 Gemini), energy dispersive X-ray spectroscopy (EDX) analysis (SEM S-4800 Hitachi) equipped with an EDX detector Quantex 200, Bruker), atomic force microscopy (AFM - Thermo Microscopes Explorer 4400–11), Raman spectroscopy (Renishaw InVia Spectroscope with 532 nm excitation wavelength), a spectrophotometer (Perkin Elmer Lambda 1050 with integrating sphere), femtosecond multicolor pump-probe spectroscopy at near infra-red spectral range and by Van der Pauw method.

3. Experimental

3.1 Morphological characterization

Figure 2 shows the scanning electron microscope (SEM) images of the fabricated carbon films. From Fig. 2a one can see that the PPF surface is homogeneous. This observation is consistent with results published in Refs.[18, 22]. The high-resolution SEM images shown in Figs 2b,c reveal that the films pyrolyzed with Ni catalyst layer have either embedded sub-micron size Ni particles (Fig. 2b, GRF(Ni+)) or holes of the same size (Fig. 2c, GRF (Ni-)). That is the melted Ni catalyst film recedes and forms micron and sub-micron size Ni particles. After removal of the Ni, by the wet etching, there is appearance of holes in the GRF where Ni particles were located. It is worth noting that both nickel particles and holes may increase the surface roughness of GRF (Ni+) and GRF (Ni-) in comparison with the PPF.
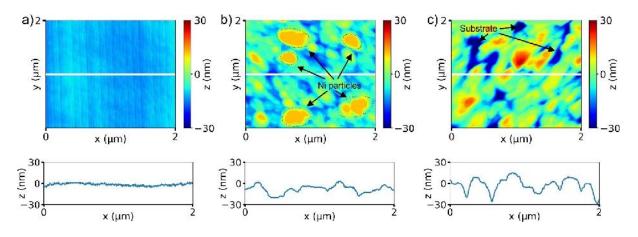

Figure 2. Scanning electron microscope images of synthetized carbon films. The PPF (a) is very homogeneous throughout the sample. The GRF(Ni+) (b) and GRF(Ni-) (c) have defects that originate from melted Ni film. (d-e) The EDX spectra of GRF(Ni+) and GRF(Ni-).

In the EDX spectra of GRF(Ni+) and GRF(Ni-) shown in Fig 2(d) and (e), respectively, one can see the peaks corresponding to C, O, Si (~0.28 eV, ~ 0.52 eV and ~1,74 eV). The absence of the

Ni peak (at 0.82 eV) in the EDX spectra of the GRF(Ni-) is consistent with results of the SEM characterization (see Fig 2c) showing that Ni particles have been mostly removed by wet etching. Moreover, it is worth noticing that the amount of oxygen in GRF(Ni-) sample is increased of about 10 %, indicating additional oxidation of GRF in the course of the oxygen plasma treatment.

The results of AFM mapping are presented in Fig. 3. In Fig. 3a one may observe vertical lines in the PPF AFM map that may originate from the spin-coating process. The thickness of the obtained PPF films is 55 nm ($\pm$2 nm). The average surface roughness (R_a) and peak-to-peak surface roughness (R_{pp}) for the PPF were about 6.5 nm and 3.3 nm, respectively, which correspond to highly smooth surface (compare with[18]).

On the contrary, surfaces of the GRF(Ni+) and GRF(Ni-) are rather rough. In the GRF(Ni+) sample, R_a and R_{pp} were 16 nm and 32 nm, respectively. The GRF(Ni-) sample had highest roughness with R_a and R_{pp} of 48 nm and 78 nm, respectively. In Fig. 3b, yellow round shapes correspond to the Ni particles resembling the SEM images in Fig. 2b. Furthermore, in Fig. 3c, one can observe flat areas, which are roughly 40 nm lower than the rest of the film. These flat areas correspond to the underlying fused silica substrate indicating that Ni particles goes fully through the GRF during the synthesis. Due to roughness, the exact thickness of GRF is difficult to define. The estimated average thicknesses for GRF(Ni+) and GRF(Ni-) were 50 nm ($\pm$ 5 nm) and 40 nm ($\pm$ 5 nm). For GRF(Ni+) the thickness was almost the same as for PPF while for GRF(Ni-) thickness is reduced due to brief oxygen etching before Ni wet etching.
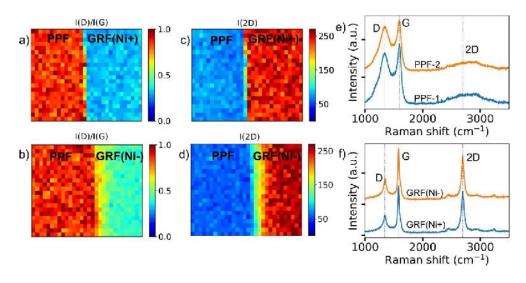
Figure 3. Height mapping done by an atomic force microscope and surface profiles. (a) The surface roughness of the PPF sample is very low in comparison with that of (b) GRF(Ni+) and (c) GRF(Ni-). (b) The height map of GRF(Ni+) sample shows peaks corresponding to Ni particles shown in SEM image. (c) After Ni etching process, the roughness of GRF(Ni-) is greatly increased due to the voids on those areas where Ni has been removed. Surface profile bellow a height map corresponds white line in the map.

3.2. Raman characterization

The fundamental D ("disorder") and G ("graphitic") peaks in Raman spectra contain information on the crystallinity of the carbon material[23, 24]. For undoped graphite, the D- and the G-peak are located at ~1350 cm⁻¹ and 1582 cm⁻¹, respectively. The D peak is activated in presence of a defect in graphite and vanishes in a defect-free graphite lattice[23, 24]. Therefore, the ratio of D- and G-peak intensities, I(D)/I(G), is used as a measure of crystalline quality of the GRF[24]. Furthermore, 2D-peak at ~2700 cm⁻¹, is a good indicator of the presence of the graphitic material since in amorphous pyrolytic carbon films this peak is strongly suppressed[25, 26]. Therefore, measurement of the I(D)/I(G) ratio and I(2D) provide information on the crystallinity of the GRF.

Figure 4 shows Raman maps of I(D)/I(G) ratio and I(2D) for PPF, GRF(Ni+) and GRF(Ni-). The I(D)/I(G) ratio of PPF is close to one inherent for strongly disordered material[26-28]. D- and G-peaks are rather wide, while full-width half maximums (FWHMs) are ~100 cm⁻¹ and ~60 cm⁻¹,

respectively, and 2D peak is hardly observable. These experimental finding indicates that PPF is highly disordered, amorphous carbon film as expected[28].

On the contrary, D, G and 2D peaks of GRF are narrow (FWHMs are about 60cm^{-1}, 35 cm^{-1} and 55 cm^{-1} respectively). For GRF(Ni+) and GRF(Ni-) the I(D)/I(G) ratio is approximately 0.4 and 0.55, respectively, which indicate that the former possesses lower disorder. Interestingly, 2D peak in both GRF(Ni+) and GRF(Ni-) is about of the same order of magnitude. Therefore the measured Raman spectra indicate that the thin Ni catalyst film greatly improves crystallinity of the pyrolyzed resist. Ni removal from the film may introduce some structural damages of the GRF though.

Figure 4. Raman characterization of PPF, GRF(Ni+) and GRF(Ni-). (a,b) The intensity ratio of D and G peaks is lower in GRF(Ni+) than that in GRF(Ni-). (c,d) The 2D peak intensity is almost equal in GRF before and after Ni removal. (e) PPF-1 and PPF-2 denote PPF before and after Ni removal, respectively, and shows that there is practically no difference in Raman spectra. (f) Raman spectra of GRF(Ni+) and GRF(Ni-) are almost identical but differ greatly from PPF.
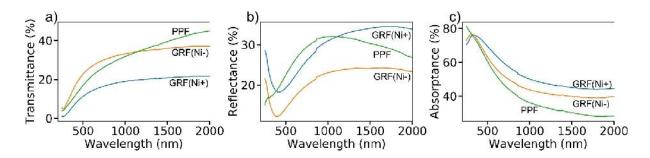
3.3 Optical characterization

In order to access the band structure of the synthesized films and thus brings the insights to the electrical properties of the material we measured the transmittance, reflectance and absorbance spectra of the synthesized films at the range of 250 to 2000 nm. Because of gapless and linear band

structure in the vicinity of the K-point of the Brillouin zone, graphene has a constant (~2.3 %) absorptance over VIS-NIR spectral range and shows an absorption peak at around 260 nm due to M-saddle point absorption[28, 29]. In a multilayered graphene, the dependence of the electron energy on the quasimomentum is not entirely linear at the Dirac point[29]. However, when moving further from the Dirac point toward higher photon energies (e.g. ~0.5 eV to 2.5 eV) the electron energy becomes almost linear function of the quasimomentum giving rise to the nearly dispersionless absorption coefficient of the multilayered graphene[28, 30].

In the experiment, we measured transmission and reflectance spectra of pyrolyzed films at the range from 250 to 2000 nm. Figure 5 shows transmittance (T), reflectance (R) and absorptance ($A=1-T-R$) spectra of PPF, GRF(Ni+) and GRF(Ni-). One can observe that PPF transmittance changes drastically over the measured spectral range, while that of GRF(Ni+) and GRF(Ni-) stays on almost constant at 18 % and 35%, respectively. The transmittance minimum for both GRF samples is located at ~260 nm, which well corresponds to the M-saddle point absorption in graphene. There exists an absorption maximum at around 325 nm in GRF, while the PPF absorption spectrum is featureless at this wavelength.

Furthermore, the GRF(Ni+) has lower transmittance and higher reflectance in comparison to those of the GRF(Ni-). This is because Ni particles reflect and scatter incident light thus increasing the extinction. Interestingly however, the absorptance spectra of GRF(Ni+) and GRF(Ni-) are similar having about only 5 % difference in the NIR range and being nearly the same at 325 nm.

Spectrophotometry shows that optical absorption of the GRF is about 20 times higher than that in graphene. However, it is even more important that the transmittance of GRF(Ni+) and GRF(Ni-) is almost constant over very wide spectral range resembling that of graphene.

Figure 5. (a) Transmittance, (b) reflectance and (c) absorptance of PPF, GRF (Ni+) and GRF (Ni-). Spectra of GRF samples synthetized with Ni catalyst shows very clear different from the amorphous PPF.
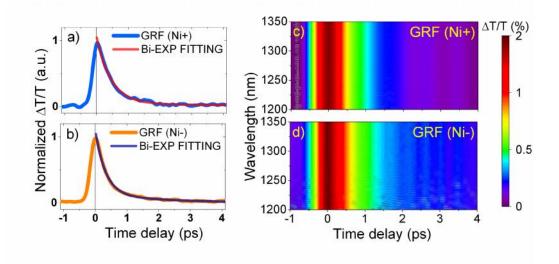
We may conclude that Raman spectroscopy and spectrophotometry indicate that synthetized GRFs are well-ordered graphitic material possessing an electron band structure similar to that of graphite and graphene.

3.4. Pump-probe experiment

We performed a pump-probe experiment with synthesized carbon films to characterize their excited states and to obtain information on the kinetics of the photoexcited carriers in the time and frequency domains[31, 32]. In time-resolved pump-probe measurements, femtosecond pulses with a central wavelength of 780 nm and a femtosecond continuum were employed as a pump and broadband probe, respectively. The pump pulses were delivered by a Ti:sapphire regenerative femtosecond amplifier (central wavelength of 780 nm, pulse duration 160 fs, repetition rate 1 kHz). The probe continuum pulses were generated by focusing the beam at the wavelength of 780 nm and with the average power of 100 mW in a sapphire crystal. The femtosecond continuum was used to probe the differential transmission ($\Delta T/T$) in a spectral range spanning from 1150 nm to 1400 nm. The pump and probe beams were collinearly polarized. In the experiment, we used 1 kHz repetition rate and fluence of about 100 $\mu J/cm^2$ at the peak irradiance of 625 MW/cm^2. It is one order of magnitude below of the level when the two-photon absorption can be observed and two orders of magnitudes lower the optical damage threshold of the GRF[17]. The time delay

between the probe and pump pulses was controlled by a rapid motorized delay line. The pump-induced change of the probe transmission was detected with an IR-spectrometer. All measurements were performed at room temperature.

The two-dimensional plots on Fig. 6 represent the differential transmittance ($\Delta T/T$) spectra of GRF(Ni+) and GRF(Ni-) samples at the 780 nm excitation as functions of pump-probe delay time. The positive $\Delta T/T$ indicates the presence of saturating absorption. Under pump fluence of 625 MW/cm^2 we observed about 1.5 % change in transmittance in both GRF(Ni+) and GRF (Ni-) samples. No pronounced $\Delta T/T$ signal was obtained from PPF in agreement with our earlier studies of amorphous carbon films[17, 33]. The biexponential fitting of normalized $\Delta T/T$ kinetics taken at 1300 nm probe wavelength revealed fast and slow components associated with intra- (T_1) and interband (T_2) relaxation: $T_1^{(Ni+)} = (450 \pm 60)$ fs , $T_1^{(Ni-)} = (320 \pm 50)$ fs and $T_2^{(Ni+)} = (2500 \pm 150)$ fs, $T_2^{(Ni-)} = (1850 \pm 120)$ fs for GRF(Ni+) and GRF(Ni-), respectively. The total relaxation (T_1+T_2) time is order of 2-3 picoseconds, which is similar to that of graphene[31, 32]. The obtained ultrafast relaxation rates agree with transient absorption dynamics obtained under similar excitation conditions in CVD multilayer graphene[31] and graphite[34].

Figure 6. Nonlinear optical characterization of GRF(Ni+) and GRF(Ni-). (a,b) The differential transmittance ($\Delta T/T$) at 625 MW/cm^2 peak irradiance and $\Delta T/T$ spectra are almost identical for

GRF(Ni+) and GRF(Ni-). The total relaxation (T_1+T_2) time is order of 2-3 picoseconds, which is similar to that of graphene. (b) Probing the sample with different wavelengths (1150 – 1250 nm) shows that the ΔT/T has no frequency dependency in this regime. Two dimensional plots of multicolour pump-probe data obtained upon excitation of (c) GRF(Ni+) and (d) GRF(Ni-) samples at 780 nm.

3.5 Carriers transport characterization

Followed by an extensive optical inspection of the synthetized carbon films, we measured electrical characteristics of fabricated samples by using the standard Van der Pauw method to obtain the carrier concentration and mobility.

Samples having area of 10x10 mm^2 with 1x1 mm^2 gold contacts at the corners were used. We performed measurements at the magnetic field strength of 0.9 T oriented parallel and anti-parallel to the sample normal. For all of the measurements, the magnitude of the injected current as well as the magnetic field strength were the same. In the experiment, we measured the voltage $V_{ij, P}$ ($V_{ij, N}$) between i-th and j-th corners of the sample at the positive (negative) direction of the magnetic field. The polarity of the Hall voltage indicates the type of material the sample is made of; it is positive for *p*-type material, and negative for the *n*-type. The overall Hall voltage $V_H = (V_{13, P} - V_{13, N} + V_{24, P} - V_{24, N} + V_{31, P} - V_{31, N} + V_{42, P} - V_{42, N})/8$ allows us to obtain mobility as follows: The resistivity was calculated as $\rho = (q(n\mu_n + p\mu_p))^{-1}$, where n and μ_n (p and μ_p) are the concentration and mobility of electrons (holes), respectively. At high doping, this equation can be reduced down to $\rho = (qn_m\mu_m)^{-1}$, where subscript "*m*" labels the majority carrier. By introducing the sheet carrier density $n_S = n_m d$ and sheet resistance $R_s = \rho/d$, where d is the film thickness, the majority carrier mobility can be presented as $\mu_m = (qn_sR_s)^{-1}$. The transport properties of PPF, GRF(Ni+) and GRF(Ni-) are summarized in Table 1.

Due to the amorphous nature of PPF, the carrier mobility was low as expected and in the same range as it has been reported earlier[35]. Moreover, the electrical conductivity of PPF was also relatively low (~15 S/cm) being of the same order of magnitude as that of other amorphous carbon materials[18], although slightly higher conductivity can be achieved by annealing PPF at elevated temperature[18, 25].

Both GRF(Ni+) and GRF(Ni-) samples show conductivity and mobility almost three orders of magnitude higher than those of the PPF. The GRF(Ni+) has higher sheet resistance than GRF(Ni-). That is the removal of the Ni particles embedded in the film results in the increase of the GRF(Ni-) conductivity due to chemical unintentional doping of the film in the course of the nickel wet etching in $CuSO_4$:HCl:H_2O solution. The similar effect of the chemical doping on electrical properties of the roll-to-roll produced graphene was reported in[36]. The doping mechanism may involve lattice defects caused by oxygen RIE and chemical doping as a result of Ni wet etching in $CuSO_4$ based solution. Because of doping, the carrier density of GRF(Ni-) is increased. This manifests itself in the lower hole mobility in comparison with GRF(Ni+) (see Table 1).

Table 1. Electrical characteristics of the synthetized carbon films.

	Sheet resistance (Ω/sq)	Thickness (nm)	Resistivity (Ω cm)	Conductivity (S/cm)	Hole mobility ($cm^2V^{-1}s^{-1}$)	Sheet carrier density (cm^{-2})	Carrier density (cm^{-3})
PPF	12500	55	70×10^{-3}	14.3	0.2	2.6×10^{15}	4.7×10^{20}
GRF(Ni+)	300	~50	$\sim1.5 \times 10^{-3}$	667	160	1.3×10^{14}	2.5×10^{19}
GRF(Ni-)	175	~40	$\sim0.7 \times 10^{-3}$	1430	90	3.9×10^{14}	9.8×10^{19}

In spite of the fact that the carrier mobility in the GRF is about two orders of magnitude lower than that in polycrystalline graphene[37] and single-crystal graphene films[38, 39], its high conductivity, advantageous optical properties and scalable fabrication make GRF a good candidate for THz applications, where the high hole mobility is not the must[40, 41].

3.6 Micropatterning

Receding of a melted metallic thin film can be controlled by modifying the substrate surface. Such a technique has been demonstrated earlier to synthetize self-organizing graphene structures on dielectric substrates[42, 43]. This approach, however, cannot be used for pyrolyzed films because relatively thick resist film deposited on the top of Ni catalyst layer reduces the mobility of Ni particles during the annealing. We propose a feasible and scalable alternative technique that enables fabrication of the graphitic circuits by pyrolysis of the pre-pattering resist layers.

Figure 7a shows a schematic illustration of the GRF microstructure fabrication. Following the preparation steps described above, we covered a silica substrate with 10 nm thick Ni film and with 350 nm thick nLOF photoresist layer. After that, we patterned the photoresist using electron beam lithography and annealed the sample at 800 °C (see section 2. Sample fabrication). After annealing, we obtained GRF microstructures embedded with Ni particles, which are shown in Fig. 7b. Ni particles are removed by dry/wet etching process (Fig. 7c) as described above.

Figure 7. (a) A schematic illustration of GRF micropattern synthesis on a fused silica substrate. Optical microscope image of microstructures (b) with Ni particles and (c) after Ni removal. (d) A GRF(Ni+) structure with 3 μm linewidth. (e) Raman spectra measured from points P1 and P2. (f,g) Raman mapping from (d) for I(D)/I(G) and for I(2D). (h) A GRF(Ni-) structure with 3 μm linewidth. (i) Raman spectra measured from points P3 and P4. (j,k) Raman mapping from (h) for I(D)/I(G) and for I(2D).

Figure 7 shows Raman mapping and Raman spectra of GRF structures with 3 μm linewidth. One can see that the patterned GRF(Ni+) and GRF(Ni-) are more disordered in comparison with continuous film having I(D)/I(G) ratio of about 0.5-0.7 in both structures. We did not observe a clear difference in I(D)/I(G) ratio between GRF(Ni+) and GRF(Ni-) as we did for continuous films. Moreover, despite the increase of I(D)/I(G) ratio (i.e. increased disordering) in GRF structures, the 2D peak was yet clearly visible in both structures. We observed that there is a very

thin layer of amorphous carbon on the outer area of microstructures. However, this carbon film fully disappeared because of oxygen RIE during the Ni removal process.

The patterning resolution is determined by the Ni particle size, and it is therefore at the level of hundreds nm. It could be reduced down to tens of nm by using e.g. magnetron sputtering, which will produce more homogeneous – in comparison with thermal evaporation - Ni layer. However, for THz applications and for fabrication of the graphitic circuits the resolution provided by thermally evaporated catalyst layers is sufficient.

4. Discussion and conclusions

Although the ultra-thin Ni catalyst film makes the carbon film rather rough, an extensive electrical and optical characterization demonstrates that the GRF outperforms PPF in terms the carrier mobility, conductivity and saturable optical absorption. A pronounced 2D peak at GRF Raman spectra as well as almost constant optical absorption in wide spectral range indicate that GRF has a similar electronic band structure to that of multilayered graphene[29,30]. This conclusion is also supported by the pump-probe optical experiment, which shows very clear, frequency independent increase in transmission after high intense pump pulse.

The optical absorption of GRF is approximately 20 times higher than that of graphene. Therefore, GRF can be employed for the fabrication of modulators or detectors of bolometric type. Moreover, the process involves metallic particles, which provide a versatile platform to study e.g. plasmonic resonances in GRF-metal particle composite.

The pump-probe experiment shows that the total carrier relaxation time is of the order of 2-3 ps. This value is very close to that recorded for single- and multilayer graphene[32], which indicates that the ultrafast carrier dynamics in GRF material is governed by the physics of the single graphene sheet. Although, the relaxation time is very similar in GRF with and without Ni, the observed interband relaxation time T_2 in GRF(Ni+) is slightly (about 500 fs) longer in comparison to that in

GRF(Ni-). This may originate from additional carrier scattering channels and charge transfer due to the presence of Ni particles.

Intuitively one may expect that a GRF with Ni particles have higher electrical conductivity vs GRF(Ni-). However, removing Ni particles clearly dopes the GRF leading to increasing conductivity of GRF(Ni-). The doping is likely caused by the oxygen plasma etching, which exposes the Ni particles and dopes GRF by adding lattice defects. This conclusion is supported by the increase in I(D)/I(G) ratio in Raman spectrum and also by slight increase of oxygen level shown by the EDX analysis. The unintentional doping reduces carrier mobility of the GRF(Ni-) but increases its conductivity.

Even though the measured in-plane carrier mobility of GRF samples was about 2-3 orders of magnitude higher than that in PPF, it is still rather low in comparison with graphene. This is expected to originate from strong disordering of GRF that results in the scattering of carriers on the boundaries of graphitic flakes. Moreover, although the synthetized GRF is nanometrically thin, one may expect that graphitic flakes comprising the film are randomly oriented. It explains why the GRF mobility is one order of magnitude less than the best values reported for graphene directly grown on dielectric support (i.e. from 1 000 to 4 000 $cm^2V^{-1}s^{-1}$)[14, 15]. However, despite the recorded mobility values for GRF are relatively low, the carrier mobility of GRF(Ni+) demonstrates comparable level with that of a few-layer graphene, synthetized directly on an insulating surface with a sacrificial Cu thin film by CVD[15]. It is also worth noticing that with the Van der Pauw measurement we recorded hole mobility and thus, one may expect that the electron mobility in GRF is slightly higher than those values shown in Table 1.

Raman characterization of GRF microstructures (see Fig. 7) with and without Ni particles shows that the GRF has higher I(D)/I(G) ratio than that of the continuous layer of GRF(Ni+). This is an indication of higher degree of disordering in GRF micropatterns. The reason for the higher disordering is assumed to originate from e-beam exposure that crosslinks polymer chains in the

resist film and thus changes the properties of the nLOF resist. To verify this assumption, we coated two silica substrates with 10 nm of Ni and 350 nm of nLOF. One sample we processed after coating, while the second one was left for two days exposed to UV-light. The sample that was exposed to UV-light showed higher I(D)/I(G) ratio than that processed right after nickel and resist coating. This supports the conclusion that exposing the resist film to the electronic or UV beam will modify the process and results material with slightly higher disordering. Due to disordering, physical properties of GRF ribbons may vary from the continuous GRF. Recovering physical properties of directly deposited GRF ribbons will be our further goal.

To summarize, our results show that pre-deposited ultra-thin Ni layer has drastic impact to physical properties of a pyrolyzed photoresist film. Their dependence on thicknesses of the Ni and photoresist layers, and the annealing conditions provides a nice playground for searching the ways to optimize the process and the fabrication routines. Since the synthesis technique is based on resist precursor, it is an appealing route to produce micron size graphitic structures as we demonstrated here. This approach can be further utilized for instance for fabrication of Ohmic contacts for graphene[44], graphitic microwires, and graphene/graphite based photonics and optoelectronic devices that require an enhanced optical absorption.

REFERENCES

[1] Nair RR, Blake P, Grigorenko AN, Novoselov KS, Booth TJ, Stauber T, Peres NMR, Geim AK. Fine Structure Constant Defines Visual Transparency of Graphene. Science 2008; 320:1308.

[2] Bonaccorso F, Sun THZ, Ferrari AC. Graphene Photonics and Optoelectronics. Nat Phot. 2010; 4(9):611–622.

[3] Obraztsov AN, Volkov AP, Nagovitsyn KS, Nishimura K, Morisawa K, Nakano Y and Hiraki A. CVD Growth and Field Emission Properties of Nanostructured Carbon Films, J. Phys. D: Appl. Phys. 2002; 35: 357–362.

[4] Bo Z, Yang Y, Chen J, Yu K, Yan J, Cen K. Plasma-Enhanced Chemical Vapor Deposition Synthesis of Vertically Oriented Graphene Nanosheets, Nanoscale 2013; 5: 5180-5204.

[5] Fang Z, Wang Y, Schlather AE, Liu Z, Ajayan PM, García de Abajo FJ, Nordlander P, Zhu X, Halas NJ. Active Tunable Absorption Enhancement with Graphene Nanodisk Arrays. Nano Lett. 2013; 14(1): 299-304.

[6] Liu JT, Liu NH, Li J, Jing Li X, Huang JH. Enhanced Absorption of Graphene with One-dimensional Photonic Crystal. App Phys Lett 2012; 101(5): 052104.

[7] Wang R, Ren X-G, Yan Z, Jiang L-J, Sha WEI, Shan G-C. Graphene Based Functional Devices: A Short Review. Frontiers of Physics 2019; 14:13603

[8] Ma J, Huang H, Ning K, Xu X, Xie G, Qian L, Loh KP, and Tang D. Generation of 30 fs Pulses from a Diode-pumped Graphene Mode-locked Yb:CaYAlO$_4$ laser. Optics Letters 2016; 41(5): 890-893

[9] Reina A, Jia X, Ho J, Nezich D, Son H, Bulovic V, Dresselhaus MS, Kong J. Large Area, Few-layer Graphene Films on Arbitrary Substrates by Chemical Vapor Deposition. Nano Lett 2009; *9*(1):30-35.

[10] Li X, Cai W, An J, Kim S, Nah J, Yang D, Piner R, Velamakanni A, Jung I, Tutuc E, Banerjee SK, Colombo L, Ruoff RS. Large-area Synthesis of High-quality and Uniform Graphene Films on Copper Foils. Science. 2009; 324(5932):1312-1314.

[11] Zhu Y, Ji H, Cheng H-M, Ruoff RS. Mass Production and Industrial Applications of Graphene Materials. Nat Sci Rev 2018; 5(1): 90-101.

[12] Chen Y, Sun J, Gao J, Du F, et al. Growing Uniform Graphene Disks and Films on Molten Glass for Heating Devices and Cell Culture. Advanced Materials 2015; 27: 7839-7846.

[13] Su CY, Lu AY, Wu CY, Li YT, Liu KK, Zhang W, Lin S-Y, Juang Z-Y, Zhong Y-L, Chen F-R, Li L-J. Direct Formation of Wafer Scale Graphene Thin Layers on Insulating Substrates by Chemical Vapor Deposition. Nano Lett 2011; 11(9):3612–3616.

[14] Kwak J, Chu JH, Choi J-K, Park S-D, Go H, Kim SY, Park K, Kim S-D, Kim Y-W, Yoon E, Kodambaka S and Kwon S-Y. Near Room-temperature Synthesis of Transfer-free Graphene Films. Nat Comm. 2012; 3: 645.

[15] Park BJ, Choi JS, Eom JH, Ha H, Kim HY, Lee S, Shin H, Yoon S-G. Defect-free Graphene Synthesized Directly at 150 °C via Chemical Vapor Deposition with no Transfer. ACS Nano 2018; 12(2): 2008-2016.

[16] Kaplas T, Matikainen A, Nuutinen T, Suvanto S, Vahimaa P, Svirko Y. Scalable Fabrication of the Graphitic Substrates for Graphene-enhanced Raman Spectroscopy. Scientific Reports 2017; 7(1):8561.

[17] Kaplas T, Babaeian M, Cromey B, Baah M, Obraztsov P, Akhoundi F, Peyghambarian N., Kieu K, Svirko Y. Strong Optical Nonlinearity of Ultrathin Graphitic Films Synthesized on Dielectric Substrates. Appl Surf Sci 2019; 497: 143766

[18] Schreiber M, Lutz T, Keeley GP, Kumar S, Boese M, Krishnamurthy S, Duesberg GS. Transparent Ultrathin Conducting Carbon Films. Appl Surf Sci 2010; 256(21):6186-6190.

[19] Yu Q, Lian J, Siriponglert S, Li H, Chen YP, Pei S-S. Graphene Segregated on Ni Surfaces and Transferred to Insulators. Appl. Phys. Lett. 2008; 93: 113103.

[20] Lander JJ, Kern HE, Bleach AL. Solubility and Diffusion Coefficient of Carbon in Nickel: Reaction Rates of Nickel-Carbon Alloys with Barium Oxide. J. App. Phys. 1952; 23:1305–1309.

[21] Li X, Cai W, Colombo L, Ruoff RS, Evolution of Graphene Growth on Ni and Cu by Carbon Isotope Labeling. Nano Lett. 2009; 9: 4268-4272

[22] Kaplas T, Kuzhir P. Ultra-thin Pyrocarbon Films as a Versatile Coating Material. Nanoscale Res Lett 2017; 12 (1):121.

[23] Ferrari AC, Basko DM. Raman Spectroscopy as a Versatile Tool for Studying the Properties of Graphene. Nat. Nanotech. 2013; 8(4):235-246.

[24] Jawhari T, Roid A, Casado J. Raman Spectroscopic Characterization of Some Commercially Available Carbon Black Materials. Carbon 1995; 33(11):1561-1565.

[25] Kaplas T, Kuzhir P. Ultra-thin Graphitic Film: Synthesis and Physical Properties. Nanoscale Res Lett 2016; 11(1):54.

[26] McEvoy N, Peltekis N, Kumar S, Rezvani E, Nolan H, Keeley GP, Blau WJ, Duesberg GS. Synthesis and Analysis of Thin Conducting Pyrolytic Carbon Films. Carbon 2012; 50(3):1216–1226.

[27] Ferrari AC, Robertson J. Raman Spectroscopy of Amorphous, Nanostructured, Diamond–like carbon, and Nanodiamond. Phil Trans R Soc Lond A. 2004; 362(1824): 2477-2512.

[28] Mak KF, Ju L, Wang F, Heinz TF. Optical Spectroscopy of Graphene: From the Far Infrared to the Ultraviolet. Solid State Comm. 2012; 152(15):1341-9.

[29] Slonczewski JC, Weiss PR. Band Structure of Graphite. Phys Rev 1958; 109(2):272.

[30] Koshino M. Stacking-dependent Optical Absorption in Multilayer Graphene. New J Phys 2013; 15(1):015010.

[31] Obraztsov PA, Chizhov PA, Kaplas T, Bukin VV, Silvennoinen M, Hsieh C-F, Konishi K, Nemoto N, Kuwata-Gonokami M. Coherent Detection of Terahertz Radiation with Optically Gated Graphene and Ultrathin Graphite ACS Photonics 2019, 6 (7) : 1780-1788.

[32] Obraztsov PA, Rybin MG, Tyurnina AV, Garnov SV, Obraztsova ED, Obraztsov AN, Svirko Y. Broadband Light-Induced Absorbance Change in Multilayer Graphene. Nano Lett. 2011, 11 (4): 1540-1545.

[33] Kaplas T, Karvonen L, Rönn J, Saleem M, Kujala S, Honkanen S, Svirko Y. Nonlinear Refraction in Semitransparent Pyrolytic Carbon Films. Opt. Mat. Express 2012; 2(12):1822–1827.

[34] Carbone F, Aubock G, Cannizzo A, Van Mourik F, Nair RR, Geim AK, Novoselov KS, Chergui M. Femtosecond Carrier Dynamics in Bulk Graphite and Graphene Paper. Chemical Physics Letters 2011; 504: 37–40

[35] Zhang J, Wang C, Chen J, Sun Y, Yan J, Zou Y. Xu W, Zhu D. The Highly Conducting Carbon Electrodes Derived from Spin-coated Polyacrylonitrile Films. Sci China Chem 2016; 59(6):672–678

[36] Bae S, Kim H, Lee Y, Xu X, Park J-S, Zheng Y, Balakrishnan J, Lei T, Kim HR, Song YI, Kim Y-J, Kim KS, Özyilmaz B, Ahn J-H, Hong B H, Iijima S. Roll-to-roll Production of 30-inch Graphene Films for Transparent Electrodes, Nature Nanotechnology 2010; 5: 574–578.

[37] Wang B, Huang M, Tao L, Lee SH, Jang A-R, Li B-W, Shin HS, Akinwande D, Ruoff RS. Support-Free Transfer of Ultrasmooth Graphene Films Facilitated by Self-Assembled Monolayers for Electronic Devices and Patterns. ACS Nano. 2016; 10: 1404-1410.

[38] Wang B, Huang M, Kim NY, Cunning BV, Huang Y, Qu D, Chen X, Jin S, Biswal M, Zhang X, Lee SH, Lim H, Yoo WJ, Lee Z, Ruoff RS. Controlled Folding of Single Crystal Graphene, Nano Letters 2017; 17: 1467-1473.

[39] Huang M, Biswal M, Park HJ, Jin S, Qu D, Hong S, Zhu Z, Qiu L, Luo D, Liu X, Yang Z, Liu Z, Huang Y, Lim H, Yoo WJ, Ding F, Wang Y, Lee Z, Ruoff RS. Highly Oriented Monolayer Graphene Grown on a Cu/Ni(111) Alloy Foil. ACS Nano 2018; 12: 6117-6127.

[40] Kuzhir PP, Paddubskaya AG; Volynets NI; Batrakov KG; Kaplas T; Lamberti P; Kotsilkova R; Lambin P. The Main Principles of Passive Devices Based on Graphene and Carbon Films in Microwave - THz Frequency Range, J. Nanophoton. 2017; 11: 032504.

[41] Tasolamprou AC, Koulouklidis AD, Daskalaki C, Mavidis CP, Kenanakis G, Deligeorgis G, Viskadourakis Z, Kuzhir P, Tzortzakis S, Kafesaki M, Economou EN, Soukoulis CM. Experimental Demonstration of Ultrafast THz Modulation in a Graphene-Based Thin Film Absorber through Negative Photoinduced Conductivity, ACS Photonics. 2019; 6: 720–727.

[42] Kaplas T, Silvennoinen M, Paivasaari K, Svirko Y. Self-assembled Two-dimensional Graphene Grating on a Dielectric Substrate, Appl. Phys. Lett. 2013; 102(21):211603.

[43] Kaplas T, Svirko Y. Self-assembled Graphene on a Dielectric Micro- and Nanostructures, Carbon 2014; 70:273-278.

[44] Leong WS, Gong H, Thong JTL, Low-Contact-Resistance Graphene Devices with Nickel-Etched-Graphene Contacts, ACS Nano 2014; 8 (1), 994–1001.

For Table of Contents Only